Characterising the New Zealand ambient seismic noise field: an oceanographic interpretation of western North Island spectra and beamforming results

Laura A. Brooks (1), John Townend (1), Peter Gerstoft (2), Stephen Bannister (3) and Lionel Carter (4)

(1) School of Geog, Env., and Earth Sciences, Victoria University of Wellington, PO Box 600, New Zealand
(2) Scripps Institution of Oceanography, University of California San Diego, La Jolla, California, USA
(3) GNS Science, Lower Hutt, New Zealand
(4) Antarctic Research Centre, Victoria University of Wellington, PO Box 600, New Zealand

ABSTRACT

Although seismometers are generally designed to record episodic events such as earthquakes and volcanic eruptions, most of the time they are actually recording ambient seismic noise. At frequencies lower than about one hertz, Rayleigh waves produced by nonlinear ocean wave processes constitute much of the ambient noise field. The seismological community has recently taken advantage of this and there is now much interest in using ambient seismic noise for purposes such as measuring surface wave velocities and thereby inferring the velocity structure of the crust and upper mantle. However, in order to account for spatio-temporal or azimuthal biases in the noise field underpinning surface wave velocities, the characteristics of the noise field itself must first be understood. This study investigates the spatial and temporal characteristics of the New Zealand ambient seismic noise field. Rayleigh waves at the ocean wave frequency are typically generated by direct ocean wave-induced pressure fluctuations at the sea floor, and Rayleigh waves at double this frequency are generated by opposing wave fields. New Zealand's geographic isolation exposes it to a particularly energetic ocean wave climate. Examples of signals generated in the oceans surrounding New Zealand are shown here in spectrograms of seismometer data, and are related to observed wind and ocean wave characteristics. Data collected on a seismometer array of up to 58 instruments in the Taranaki region (western North Island) were beamformed in order to estimate the relative source directions of incoming seismic noise. Signals with phase velocities corresponding to those expected for both fundamental and higher-order Rayleigh waves are observed. Regions of ambient seismic noise generation highlighted by the beamformer output are shown to agree well with modelled shallow-water (50 m isobath) ocean wave heights from around the New Zealand coast.

INTRODUCTION

Ambient seismic noise, which is predominantly observed at frequencies lower than 1 Hz, results from Rayleigh waves produced by nonlinear wave processes in the ocean [Bromirski and Duennebier (2002)]. The seismological community has recently taken advantage of this and there is now much interest in using ambient seismic noise, or 'microseisms', for estimating surface wave velocities and structural information from the crust and uppermost mantle [Weaver (2005), Sabra et al. (2005), Bensen et al. (2007), Yang et al. (2007)]. However, in order to fully account for spatio-temporal or azimuthal biases in the noise field underpinning surface wave studies, the characteristics of the noise field itself must first be identified and understood.

The microseism spectrum generally exhibits a small peak at approximately 0.06–0.07 Hz and a larger peak at 0.12–0.15 Hz, termed the single frequency (SF) and double frequency (DF) microseism peaks, respectively [Hasselmann (1963), Webb (1998)]. The SF peak is generally presumed to be generated by direct ocean wave-induced pressure fluctuations at the sea floor, the amplitude of which decrease with ocean depth [Bromirski and Duennebier (2002)]. As such, SF microseisms represent a shallow water phenomenon. The DF peak occurs due to the nonlinear interaction of opposing wavefields of similar wavenumber [Longuet-Higgins (1950)], which creates an excitation pulse at twice the ocean wave frequency that propagates almost unattenuated to the seafloor and couples into a Rayleigh wave. The minimal attenuation in the water column means that DF signals represent both shallow and deep water phenomena, though DF signals recorded on land are generally seen to be dominated by Rayleigh waves excited in shallow water regions [Haubrich and McCamy (1969), Bromirski and Duennebier (1999), Stehly et al. (2006), Tanimoto (2007)].

New Zealand is geographically isolated, exposing it to high-amplitude waves from oceanic storms, particularly those that develop in areas of the Southern Ocean south of Australia. Interaction between these large waves and New Zealand's ∼15,000 km-long coastline produces a high-amplitude seismic noise field [Pickrill and Mitchell (1979), Gorman et al. (2003)]. Researchers from the University of Auckland have previously published several ambient noise studies of the New Zealand region [Ewans (1984), Kibblewhite and Ewans (1985), Tindle and Murphy (1999)]. Kibblewhite and Ewans undertook an extensive analysis of ambient noise spectra, in particular microseisms at primary and double ocean swell frequencies, and related these to wave spectra. Tindle and Murphy studied microseisms recorded on an instrument in the basement of the physics building at the University of Auckland. They showed that the total amplitude within the microseism bandwidth was highly correlated with nearby ocean wave heights.

Ambient noise seismic tomography studies are particularly suited to regions with energetic noise fields. Taking only noise field amplitudes into consideration, New Zealand would seem an ideal candidate for such studies (Lin et al. 2007). However, due to its long coastline and complex ocean regime, New Zealand's noise field is far more spatially and temporally complex than observed in many continental regions. It is important to understand the noise field's spatio-temporal characteristics so as to ensure that ambient noise-derived wavespeed estimates within the region are accurate (Behr et al. 2009).

Beamforming involves the estimation of source location via signal processing of an array of receivers in either the time or

frequency domain. Frequency domain beamforming techniques have successfully been applied to locate oceanic seismic sources in continental regions such as Europe (Friedrich et al. 1998) and California (Gerstoft et al. 2006), but not in New Zealand.

In this paper we analyse vertical-component seismic data collected on an array in the Taranaki region, western North Island (see Fig. 1) during 2002. Our analysis includes:

- a description of the data collected;
- example month-long (July) spectrograms of the data, analysed alongside nearby wind speeds;
- a description of the beamforming methodology used to determine locations of microseism generation;
- example hour-long beamformed results;
- beamformer results for the entire month of July;
- local mean significant wave heights for the entire month of July (supplied by the National Institute of Water and Atmospheric Research from their wave prediction model, NIWAM); and
- global significant wave height snapshots (data from NOAA WAVEWATCH III hindcastsTolman (2005)) for four time periods throughout the month.

The relationship between the seismic, atmospheric (wind) and oceanographic data is shown to be strong through the various analyses presented in this paper.

DATA COLLECTION

The seismic data considered here are a sub-set of the data collected on a 61-element broadband three-component seismograph array during 2002. The array was located in the Taranaki region [Fig. 1; Sherburn and White (2005)]. Here we consider only vertical-component data for the month of July. During this period, between 50 and 58 seismographs were successfully recording data at any one time. Wind data, which were originally recorded at the New Plymouth wind station, have been obtained from the NIWA Climate Database (CliFlo). The local wave data used here are three-hourly normalised modelled wave heights (courtesy of NIWA) from 60 evenly spaced locations along New Zealand's 50 m isobath. The global wave data were sourced from WAVEWATCH III (See Acknowledgements for WAVEWATCH and CliFlo URLs).

SPECTROGRAMS

Spectrograms of data recorded during July at stations ALBT and WAST [locations shown in Fig. 1(b)] are shown in Fig. 2(a)–(b). Figure 2(c) shows the hourly wind speed at ground level recorded at the New Plymouth wind station [location shown in Fig. 1(b)] during this period. Each spectrogram data point signifies the maximum signal in the horizontal direction (that is, a vector summation of the north and east components). The data are normalised at each frequency by the median amplitude (on a logarithmic scale) at that frequency over the entire month, so that amplitude variations at all frequencies, and not just those of highest amplitude, are observed.

Due to the close proximity of the two stations (61 km) the two spectrograms appear almost identical. The most noticeable difference is the observation of SF signals at station WAST (e.g., signals of frequencies up to 0.1 Hz on days 12 and 23), but not at station ALBT. This is possibly because ALBT is further inland [see Fig. 1(b)], and therefore the relatively low-amplitude SF signals are attenuated more before arriving at this station.

Both spectrograms show low-frequency signals (<0.02 Hz) with regular periodicities of about one day; we attribute these to tidal effects. The DF spectrum above 0.1 Hz is split into two distinct portions, a set of signals between about 0.1 and 0.2 Hz, termed the long period double frequency (LPDF) signals, and

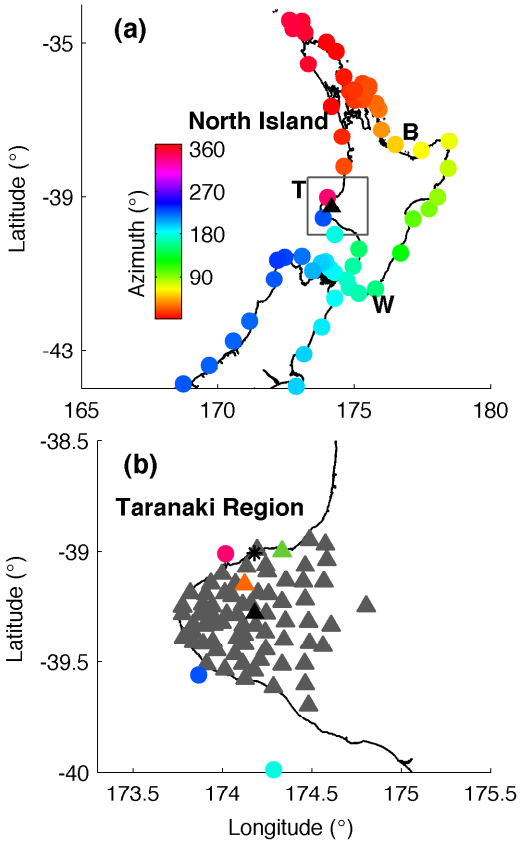

Figure 1: Map of (a) northern New Zealand and (b) the Taranaki region showing the seismic array centre location (black triangle), individual seismic stations [grey triangles except stations ALBT (orange) and WAST (green)], and locations along New Zealand's 50 m isobath at which NIWAM model wave statistics were extracted (circles coloured according to azimuth relative to the array centre). The letters 'B', 'T' and 'W' denote the Bay of Plenty, the Taranaki region, and the Wairarapa region, respectively. The black asterisk in (b) denotes the location of the New Plymouth wind station.

a set of signals above about 0.2 Hz, termed the short period double frequency (SPDF) signals. LPDF signals are generated by longer-period swell from distant storms, whilst SPDF signals are generated by shorter-period waves induced by 'local' (in this case meaning within the general vicinity of New Zealand) winds [Bromirski et al. (2005)]. As expected, the SPDF spectra amplitudes in Figs. 2(a)–(b) show strong correlations to wind speeds recorded nearby [Fig. 2(c)]. The swell-induced LPDF spectra amplitudes do not correlate well to local wind conditions. These signal peaks correspond better to times when waves from larger distant (generally Southern Ocean) storms impinge on New Zealand (observed from NOAA WAVEWATCH III).

BEAMFORMING METHODOLOGY

The seismic data were originally sampled at 5 Hz. Day-long segments were bandpass-filtered to the frequency range of interest (0.02–0.4 Hz), and downsampled to 1 Hz. The data were then separated in to 3-hour-long segments (so as to be the same period as the wave statistics), which were time domain normalised by clipping to half their standard deviation. The data were split into 128-s-long time series and Fourier transformed. The signals within each 0.008 Hz-wide band were normalised by their amplitudes. This resulted in only phase, and not amplitude, information being retained. The trace clipping and amplitude normalisation were performed to reduce the effect of episodic

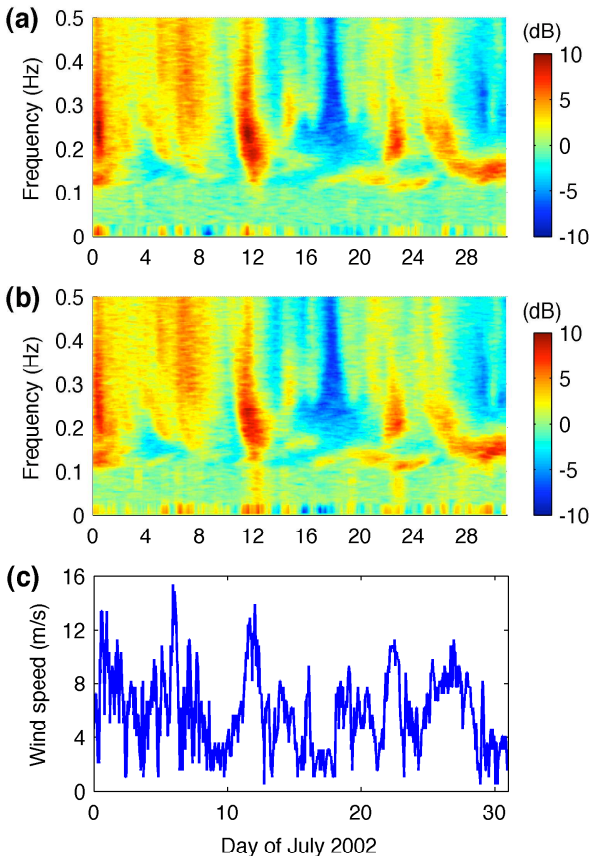

Figure 2: Normalised microseism spectra for stations (a) ALBT and (b) WAST. (c) Ground level wind speed recorded at the New Plymouth wind station.

processes such as earthquakes (Gerstoft et al. 2008, Brooks et al. 2009). Since all stations had the same nominal response, we did not make corrections for instrument response.

The pre-processed data were then beamformed. The plane wave frequency domain beamforming algorithm used here is almost identical to that described in detail in Brooks et al. (2009), the only difference being that since the original signal bandwidth is here much greater (which reduces the size of the data set), summation of the beamformed output across several frequencies was unnecessary. The array plane-wave response was determined to be acceptable for various propagation angles and frequencies within the given bandwidth (Brooks et al. 2009).

BEAMFORMING RESULTS

Beamformed outputs from 09:00–10:00 July 30 are shown in Figures 3(a)–(c) for three frequencies: 0.148, 0.164, and 0.180 Hz. Strong signals with a phase velocity of ∼2.5 km/s are observed in the south-west and south-east quadrants of Fig. 3(a). These signals are also observed in the higher-frequency Fig. 3(b) results, though it should be noted that their phase velocities have decreased to just above 2 km/s, suggesting that the signals are dispersive. The beamformer results at all three frequencies [Figs. 3(a), (b) and (c)] also show a higher-velocity signal, dominant in the south to south-west region. The phase velocity of this higher-velocity signal also appears dispersive, decreasing from about 4 km/s at 0.148 Hz to just over 3.5 km/s at 0.180 Hz.

Figure 4(a) shows the phase velocities corresponding to the maximum beamformer output, plotted as functions of time and frequency, for the entire month of July (Brooks et al. 2009). A lower-velocity (<3 km/s) dispersive signal is observed between 0.11–0.19 Hz (cyan through blue), and a higher-velocity (>3 km/s) dispersive signal is observed from ∼0.15–0.25 Hz (red through light green). The dispersion characteristics of these two distinct signals match well with fundamental and first-order Rayleigh waves respectively (Brooks et al. 2009).

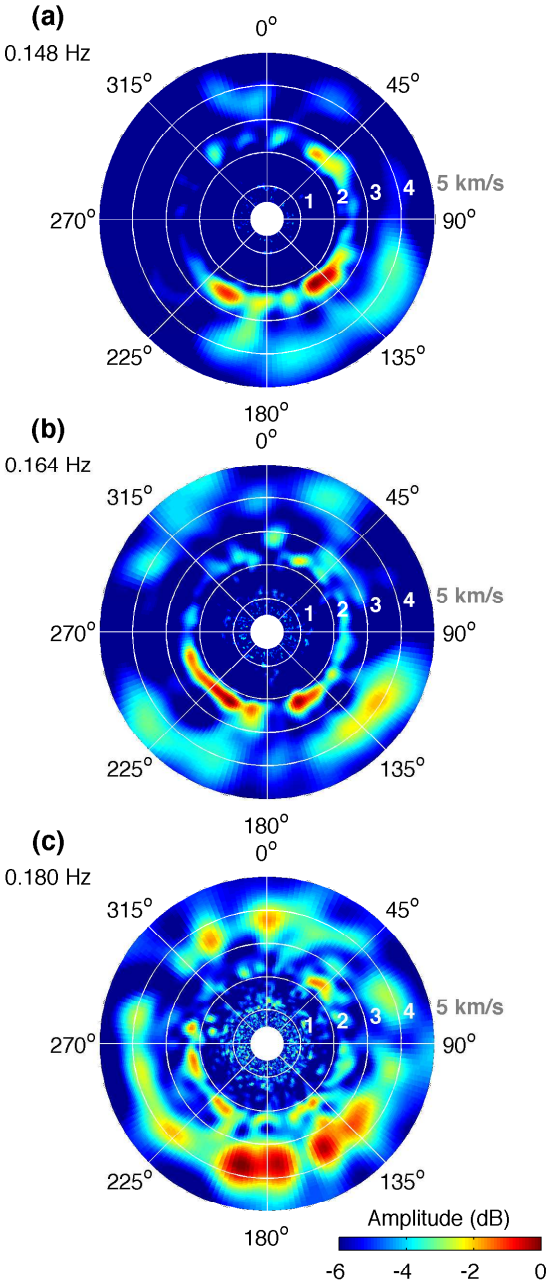

Figure 3: Beamformer outputs at (a) 0.148, (b) 0.164, and (c) 0.180 Hz from 09:00–10:00 July 30. The angular and radial axes are source azimuth from the array centre and seismic phase velocity (km/s), respectively.

Figure 4(b) shows the azimuths corresponding to the maximum beamformer output plotted throughout the month of July as a function of frequency [i.e., the azimuths corresponding to the phase velocities in Fig. 4(a)], and the normalised 50 m isobath NIWAM model wave heights for the same time period are shown in Fig. 4(c). The mean of each trace is zeroed on the azimuth of the wave site location relative to the array centre, and coloured according to the azimuth of each location (see Fig. 1). Figure 4(b) reveals that seismic noise is generated at preferred azimuths: the beamformer output is often maximum

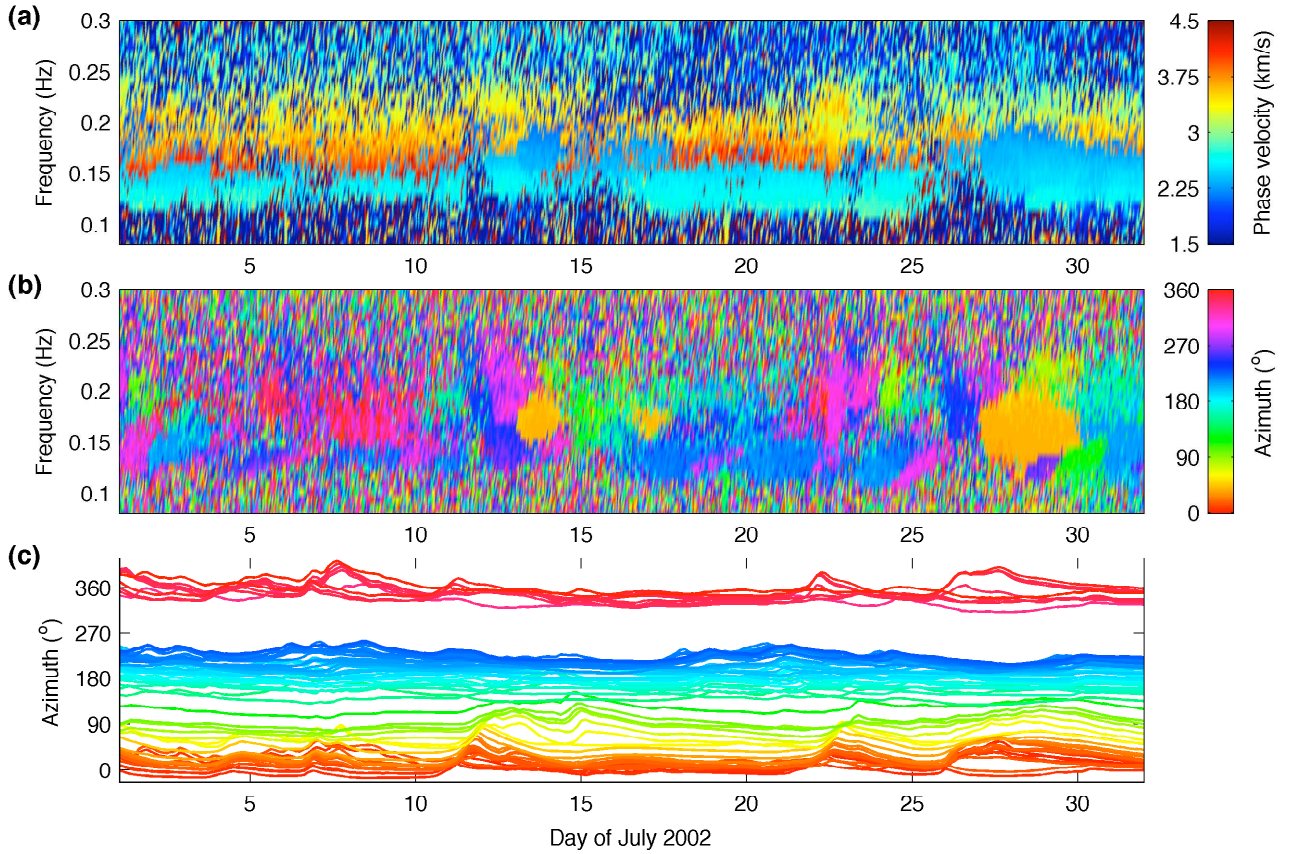

Figure 4: [Adapted from Brooks et al. (2009)] (a) Azimuths and (b) phase velocities corresponding to the maximum beamformer outputs as a function of frequency throughout July. (c) The wave heights at each NIWAM model data location circled in Fig. 1 for July.

for signals from the south and east, which is not surprising since waves from Southern Ocean storms will regularly impinge on these regions, especially during winter months. On occasions, the azimuth is, however, maximum for the (orange) Bay of Plenty and (green) Wairarapa region (both labelled in Fig. 1). It is possible that storms passing these regions create such large-amplitude signals due to both these regions having deep-water waves that progress onto a narrow continental shelf backed by a linear or semi-linear coast.

Examination of the maximum beamformer azimuths for July 30 in Figure 4(b) show a SE–SW dominance at lower frequencies (∼0.11–0.17 Hz), and a S–SE dominance at higher frequencies (∼0.17–0.24 Hz), which is what was observed in the one hour beamformer outputs of Figure 4(b).

A detailed discussion of the relationship between the seismic and wave results of Fig. 4 has been presented by Brooks et al. (2009) and will therefore not be repeated here. An important point to emphasise, however, is that peak beamformer outputs occur at azimuths that match well the azimuths of large wave heights observed a day earlier, supporting the hypothesis that the seismic signals we observe are created by near-shore ocean wave processes. We can conclude that wave heights and seismic amplitudes are related without using beamformed data simply by comparing the wave heights of Fig. 4(c) with the Fig. 2 single station spectrograms. Throughout the month, it is apparent that at frequencies above about 0.1 Hz the microseism spectra peak at times when wave heights are large. Nevertheless, the beamformed data provide an indication of the azimuth of the seismic sources, and hence provide more insight than the spectrograms alone.

Hindcasts of significant wave heights from four 3-hour intervals in July 2002 are shown in Fig. 5. Storms adjacent to New Zealand are observed (a) NW, (b) NE, (c) at the southern tip, and (d) NE of New Zealand. Consider in more detail the storm tracking across the North-East of New Zealand on July 13 [Fig. 5(b)]. Large waves from this storm are observed in the NIWAM model statistics of Fig. 4(c) at locations along the 50 m isobath between 0 and 90°. The beamformer azimuths in Fig. 4(b) successfully track this storm as it moves from East to West: the beamformer peaks in the northwest quadrant (pink) on July 13 and then in the northeast quadrant (orange) on July 14. Likewise, for the other three storms shown in Fig. 4, the direction of the storm matches well the azimuths corresponding to the beamformer peaks in Fig. 4, further supporting the correlation between wave heights and microseisms.

CONCLUSION

This analysis provides new insight into the spatio-temporal characteristics of the New Zealand noise field. Spectrograms of data from two stations show peaks in lower-frequency DF signals that correspond well to times when waves from large storms impinge on New Zealand, and the amplitudes of the higher-frequency double frequency signals correlate well to local wind speeds.

Comparison of seismic array beamformer outputs with local wave heights and global storm patterns reveal a strong relationship between ocean wave heights and microseism generation. The data and comparisons presented here have increased our understanding of microseism/ocean wave relationships and identified dominant microseism source regions, an important step in characterising the New Zealand ambient seismic noise field as a whole.

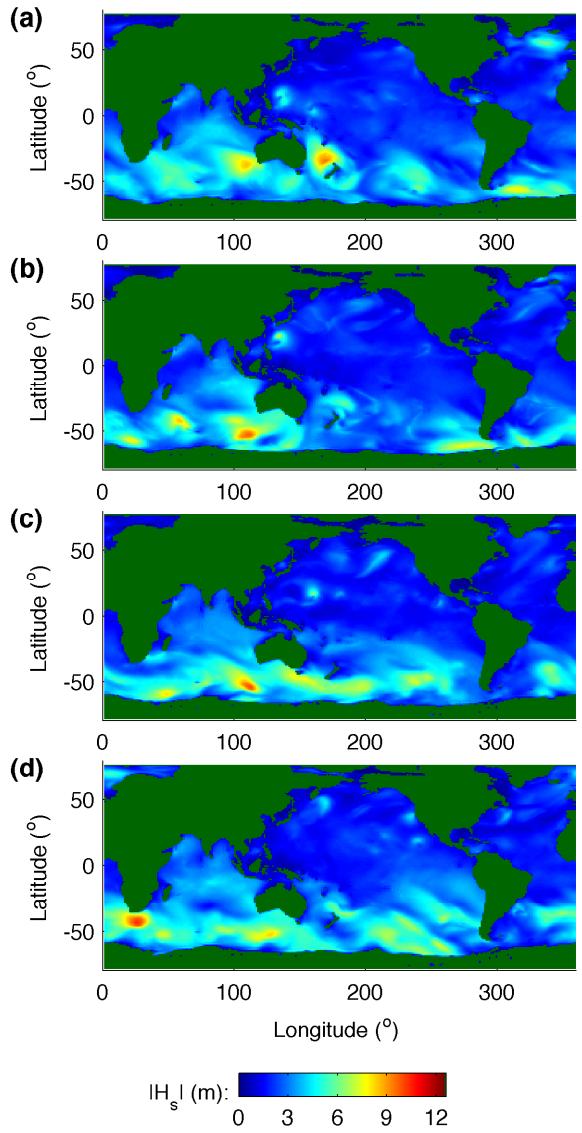

Figure 5: Hindcasts of significant wave heights for 3-hour periods commencing: (a) July 1 - 0:00GMT, (b) July 13 - 18:00GMT, (c) July 20 - 9:00GMT, and (d) July 28 - 6:00GMT.

ACKNOWLEDGEMENTS

This work was supported by the Royal Society of New Zealand's Marsden fund. The seismic data were downloaded from the IRIS Data Management Center. New Zealand wave model data were supplied by Richard Gorman, National Institute of Water and Atmospheric Research. The significant wave heights illustrate in Fig. 5 were downloaded from archived National Oceanic and Atmospheric Administration WAVEWATCH III v. 2.22 hindcast reanalysis (ftp://polar.ncep.noaa.gov/pub/history/waves). Wind data were sourced from the NIWA Climate Database, CliFlo (http://cliflo.niwa.co.nz/).

REFERENCES

Y Behr, J Townend, S Bannister, and M K Savage. Shear-velocity structure of the Northland Peninsula, New Zealand, inferred from ambient noise correlations. *J. Geophys. Res.*, under review, 2009.

G D Bensen, M H Ritzwoller, M P Barmin, A L Levshin, F Lin, M P Moschetti, N M Shapiro, and Y Yang. Processing seismic ambient noise data to obtain reliable broad-band surface wave dispersion measurements. *Geophys. J. Int.*, 169:1239–1260, 2007.

P D Bromirski and F K Duennebier. Ocean wave height determined from inland seismometer data: Implications for investigating wave climate change in the NE Pacific. *J. Geophys. Res.*, 104(C9):20,753–20,766, 1999.

P D Bromirski and F K Duennebier. The near-coastal microseism spectrum: spatial and temporal wave climate relationships. *J. Geophys. Res.*, 107(B8):2166, 2002.

P D Bromirski, F K Duennebier, and R A Stephen. Mid-ocean microseisms. *Geochem. Geophys. Geosyst.*, 6:Q04009, 2005.

L A Brooks, J Townend, P Gerstoft, S Bannister, and L Carter. Fundamental and higher-mode Rayleigh wave characteristics of ambient seismic noise in New Zealand. *Geophys. Res. Lett.*, under review, 2009.

K C Ewans. *Ocean waves, microseisms and their interrelations a study based on observations made at various locations in the New Zealand region*. PhD thesis, University of Auckland, 1984.

A Friedrich, F Krüger, and K Klinge. Ocean-generated microseismic noise located with the Gräfenberg array. *J. Seimolog.*, 2:47–64, 1998.

P Gerstoft, M C Fehler, and K G Sabra. When Katrina hit California. *Geophys. Res. Lett.*, 33:L17308, 2006.

P Gerstoft, P M Shearer, N Harmon, and J Zhang. Global P, PP, and PKP wave microseisms observed from distant storms. *Geophys. Res. Lett.*, 35:L23306, 2008.

R M Gorman, K R Bryan, and A K Laing. Wave hindcast for the New Zealand region: deep-water wave climate. *NZ J. Mar. Fresh. Res.*, 37:589–612, 2003.

K Hasselmann. A statistical analysis of the generation of microseisms. *Rev. Geophys.*, 1:177–209, 1963.

R A Haubrich and K McCamy. Microseisms: coastal and pelagic sources. *Bull. Seism. Soc. Am.*, 7:539–571, 1969.

A C Kibblewhite and K C Ewans. Wave–wave interactions, microseisms, and infrasonic ambient noise in the ocean. *J. Acoust. Soc. Am.*, 78:981–994, 1985.

F-C Lin, M H Ritzwoller, J Townend, S Bannister, and M K Savage. Ambient noise Rayleigh wave tomography of New Zealand. *Geophys. J. Int.*, 170(2):649–666, August 2007.

M S Longuet-Higgins. A theory of the origin of microseisms. *Philos. Trans. R. Soc. London, Ser. A*, 243:1–35, 1950.

R A Pickrill and J S Mitchell. Ocean wave characteristics around New Zealand. *NZ J. Mar. Fresh. Res.*, 13:501–520, 1979.

K G Sabra, P Gerstoft, P Roux, W A Kuperman, and M C Fehler. Surface wave tomography from microseisms in Southern California. *Geophys. Res. Lett.*, 32:L14311, 2005.

S Sherburn and R S White. Crustal seismicity in Taranaki, New Zealand using accurate hypocentres from a dense network. *Geophys. J. Int.*, 162:494–506, 2005.

L Stehly, M Campillo, and N M Shapiro. A study of the seismic noise from its long-range correlation properties. *J. Geophys. Res.*, 111:B10306, 2006.

T Tanimoto. Excitation of microseisms. *Geophys. Res. Lett.*, 34:L05308, 2007.

C T Tindle and M J Murphy. Microseisms and ocean wave measurements. *IEEE J. Ocean. Eng.*, 24(1):112–115, January 1999.

H L Tolman. *User manual and system doumentation of WAVEWATCH-III version 2.22*. NOAA/NWS/NCEP/OMB Technical Note 222, 2005.

R L Weaver. Information from seismic noise. *Science*, 307: 1568–1569, March 2005.

S C Webb. Broadband seismology and noise under the ocean. *Rev. Geophys.*, 36:105–142, 1998.

Y Yang, M H Ritzwoller, A L Levshin, and N M Shapiro. Ambient noise Rayleigh wave tomography across Europe. *Geophys. J. Int.*, 168:259–274, 2007.